

Partial fulfillment of DiVincenzo criteria using manipulation of Rb atomic beam

D. Khalid¹, H. O. Majeed¹ and H. Munro²

¹*Department of Physics, College of Education, Old campus, University of Sulaimani, P.O. Box 334, Sulaimani, Iraq*

²*Department of Physics, University of Leeds, LS2 9JT, Leeds, UK.*

E-mail: dastan.khalid@univsul.edu.iq

Received 02 November 2016

Abstract. We present a detailed experimental setup on the partial fulfillment of the DiVincenzo criteria. We show the necessary conditions for the experimental setup and provide a simple alternative source of an atomic beam as opposed to a complex oven system. Further simplification is provided via the negation of complex feedback-stabilization systems for the lasers used in the experiment specifically that scanning a laser with a narrow bandwidth of 70 MHz and using a fast scanning frequency around a specific transition provides significant simplification. We also found using a tuning fork chopper enhances the signal to noise ratio and introduces a further advantage and ease of setup to the experiment. The inability of interacting with multiple qubits within the experiential and thus creating a universal quantum gate is the limiting factor for not realizing all the criteria needed for a viable quantum computer..

Keywords: Atomic beam experiment, qubit manipulation, coherent control

1. Introduction

Quantum computers are one class of next generation computers, which are currently under development. Although the exact boundary of their power is still unknown they promise an exponential decrease in computing time for a range of computational problems [1].

As the name suggests processing information is based on the quantum mechanical treatment of the systems used, namely the quantum bit or qubit. Physically, any two-level quantum system can be used as a qubit where the two levels are defined as the $|0\rangle$ and $|1\rangle$ computational states respectively, the information is then encoded in the overall quantum state the system occupies. The definition of these orthogonal $|0\rangle$ and $|1\rangle$ states is analogous to the classical bit, within which the opposing states are usually represented by a change in an electrical voltage. However, unlike their classical counterpart, single qubits have a range of valid information states where they can simultaneously occupy both computational states. There is an infinite number of superposition states available that a single qubit can occupy at any one time. It is this spectrum of states together with the purely quantum phenomena of entanglement from which quantum computers draw their power. From superposition alone, it is possible for a set of n qubits to represent all 2^n combinations of n classical bits simultaneously.

In his 2000 paper, David DiVincenzo put forward five criteria he deemed necessary for any successful quantum computer [2]. To be viably scalable he stated a quantum computer would need:

- I. Qubits; a source of well characterized states that can be treated as qubits.
- II. Initialization; the ability to initialize the state of the qubits to a simple fiducial state, such as $|0000\dots\rangle$
- III. Coherence; stable and long qubit coherence time with respect to computational time scales
- IV. State manipulation; a universal set of quantum gates achieved through different qubit state manipulations.

V. State detection; qubit-specific measurement capability to read out the final state

In this paper, we discuss an experiment capable of achieving four and a half of these five criteria by implementing a basic quantum circuit as shown in Fig 1. The only limitation is that, while we have the means to perform single qubit state manipulation, we have yet no method of interacting with multiple qubit states and therefore we cannot implement a universal set of quantum gates.

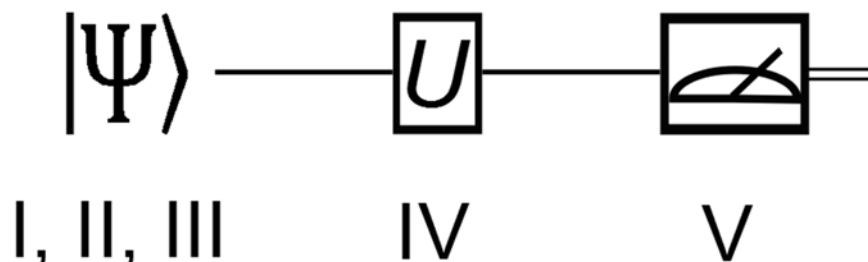


Figure 1. Diagram showing the most basic quantum circuit. A single qubit in state $|\Psi\rangle$ which corresponds to condition I, II and III of the DiVincenzo criteria is taken as input, the unitary operation U which relates to the IV criteria is performed and a measurement is made on a given basis which is equivalent to condition V.

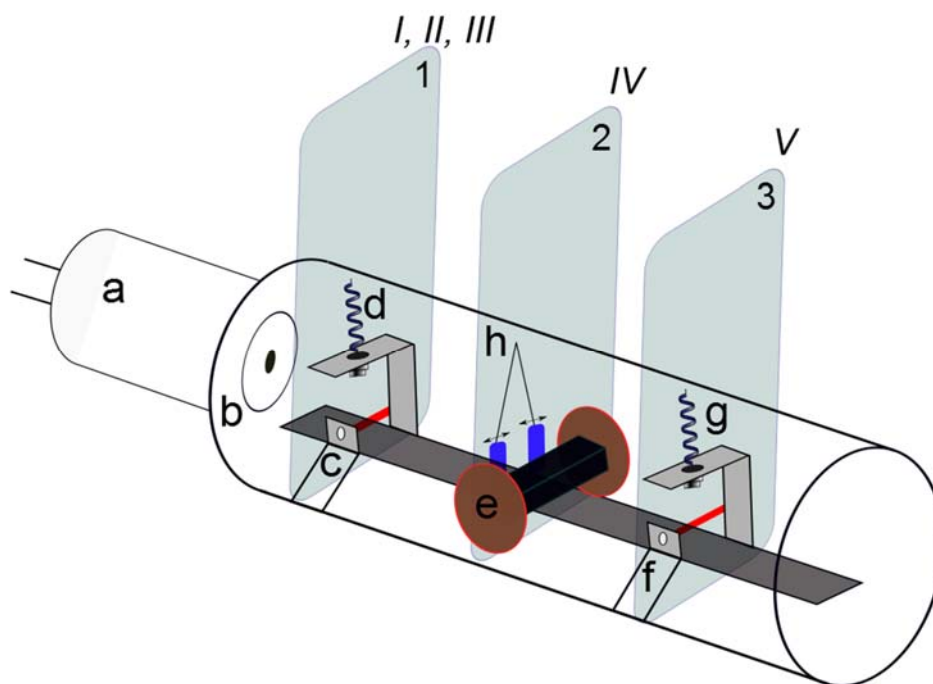


Figure 2. Schematic diagram of the experimental setup. a: small vacuum chamber where *Rb* dispenser is housed, b: collimator, c: 795 nm initialization laser through a fiber launch, d: 795 nm fluorescence detecting photodiode with a rise/fall time of $\approx 10^{-6}$ s, e: 6.8 GHz microwave waveguide which has a hole at its center so that atoms can pass through the waveguide, f: 780 nm detection laser through a fiber launch, g: 780 fluorescence detecting photodiode and h: tuning fork chopper. Region 1 (highlighted light blue rectangle): state preparation and initialization, Region 2: State manipulation and Region 3: state detection. The whole setup is evacuated to 10^{-7} mBar. The capital Roman numeric labels are the equivalence to the quantum circuit of Fig. 1 and the criteria discussed in previous sections.

2. Method

Experimental realization of the DiVincenzo criteria and thus creating the quantum circuit shown in Fig. 1 requires the following (these are presented in numerical orders for ease of comparison to the criteria presented in the introduction section).

- I. An atomic beam composed of suitable atoms to be used as qubits. To fulfill this, we have used rubidium *Rb* atoms in natural abundance. The choice of the atoms is based on the atom having a suitable transition which is stable enough to ensure coherence, for this reason, we used the ^{87}Rb ground state to-from $F = 1, 2$ (where F is the total atomic angular momentum).
- II. A laser capable of initializing the atoms into a single qubit state. Here a $\approx 795 \text{ nm}$ external cavity diode laser (ECDL) which corresponds to D_1 line of *Rb* has been used.
- III. A resonant field to excite the direct transition between the qubit states. For the atomic beam chosen in this experiment, this means a $\approx 6.834 \text{ GHz}$ microwave field, which is housed within a section of a waveguide. This specific value in microwave frequency corresponds to the energy difference between $F = 1$ and $F = 2$ of ^{87}Rb ground state.
- IV. A second laser capable of exciting the atoms from a single qubit state as a method of state detection. This is a $\approx 780 \text{ nm}$ laser (also an ECDL) which corresponds to the D_2 line of *Rb* atom.

The experimental setup is shown in Fig. 2, where the atoms are released in a forward direction into a small chamber shown in Fig.2 (a). The atoms form a well-collimated atomic beam when they travel through a 2 mm in diameter pin hole which is found at the entrance of the main chamber at (b). The collimated beam then interacted with diode laser having a wavelength of $\approx 795 \text{ nm}$ as shown by region 1 of Fig. 2. After this initial interaction, the atomic beam travels further down the main chamber to go through a microwave cavity of width 34.9 mm. A small hole is found in the cavity for the atoms to pass through at region 2 of Fig.2. The beam reaches the final stage of the setup in region 3, where they interact with another diode laser having a wavelength of $\approx 780 \text{ nm}$. The three regions are well aligned using a laser pen in the direction of region 3 from the collimator so that, the atomic beam can travel down the chamber with minimum decoherence due to collisions with various parts found in the chamber.

3. Result and Discussion

The experimental result is presented in a manner that follows the main criteria discussed in the previous sections. Except for experimental reasons, we discuss state detection (which corresponds to V of the criteria mentioned above) before state manipulation (corresponding to IV), which we will be discussed the last.

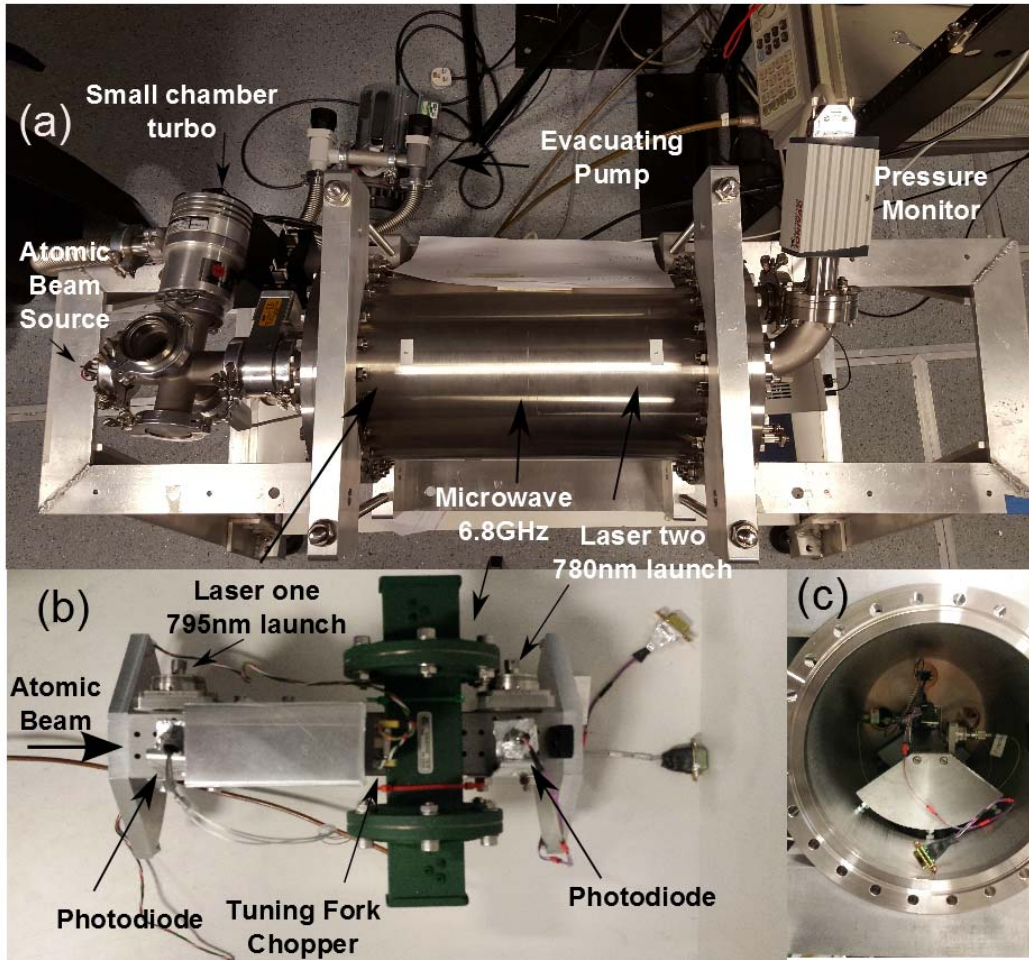


Figure 3. Actual picture of the experimental apparatus. (a) Complete setup in working condition, the pressure sensor at the end provides real-time pressure readings within the chamber. The two chambers are evacuated via the use of an evacuating pump and a pressure of 10^{-7} mBar can be reached within two hours with the aid of two turbos, one for each chamber. (b) The two lasers, microwave and the tuning fork chopper layout. (c) Cross section of the chamber where the laser-microwave component is added. The length and height of the whole experimental setup (excluding the optical setup) are 80 cm by 60 cm respectively.

A. Qubits (Atomic Beam)

The qubit is based on the electronic $5^2S_{1/2}$ ground state of ^{87}Rb . This state is split via hyperfine coupling into two distinct states with corresponding total atomic angular momentums $F = 1$ and $F = 2$. These electronic states are separated by a frequency of 6.835 GHz and are defined as the $|0\rangle$ and $|1\rangle$ qubit states respectively. Within this experiment, the rubidium atoms (the qubits) are confined within an atomic beam, which traverses the experimental vacuum chamber. To create the atomic beam, rubidium atoms are released from a SAES Getters alkali metal dispenser with a peak velocity ≈ 55 m/s (this is the peak value of the velocity distribution, which follows a Maxwellian velocity distribution). These sources consist of a folded metal container in which a powder of the stable compound rubidium chromate is housed. Both stable isotopes ^{85}Rb and ^{87}Rb are found within these sources in their natural abundance, 72% and 28%, respectively. A current of 5A is passed across the container to initiate a heat triggered reduction reaction, which results in the release of an atomic rubidium vapor, which is collimated into a beam when passing through a beam collimator (Fig.2 b). The rubidium sources have finite lifetimes according to current passed across them, this can be seen from Fig 4.

Due to their relatively short lifetimes, the sources are mounted in a smaller vacuum chamber, which is isolatable from the main interaction chamber (region *a* of Fig 2). This allows the source to be changed quickly upon exhaustion whilst maintaining the vacuum conditions in the main interaction chamber. Upon replacement it is necessary to warm up the new source slowly, this is to avoid flooding the main chamber with the exhaust gases given off by the first stages of heating. This warming up can be achieved by increasing the current to the operational current (5A) over the period of an hour. After the initial heating procedure, the sources have favorable turn on characteristics and are able to produce a stable atomic beam in under 40 seconds upon loading of the operational current.

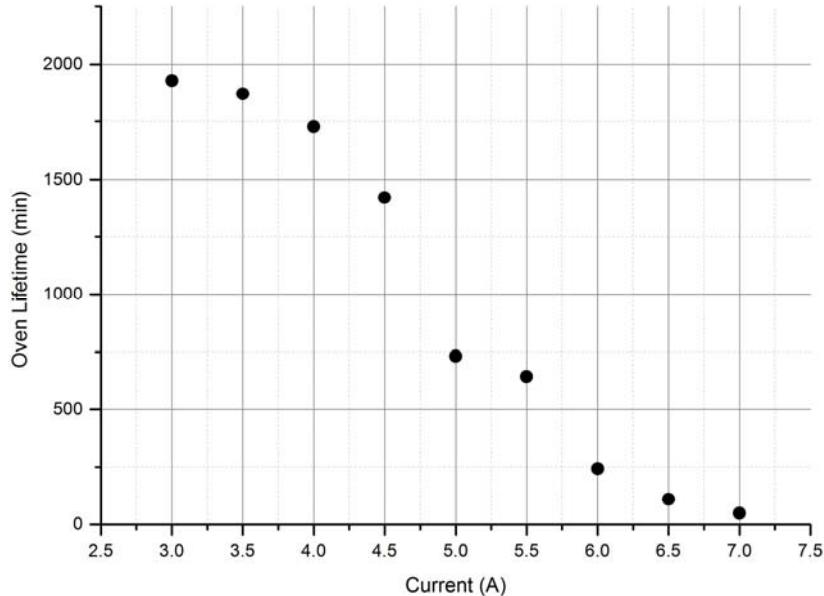


Figure 4. Lifetime for which the Rb dispenser can produce a suitable atomic beam as a function of loaded current. The measurement was made when individual dispenser was exhausted at given current.

The experiment and the subsequent observation was carried out on ^{87}Rb even though this isotope has a lower abundance as compared to ^{85}Rb . This is mainly because of the clock transition of ^{87}Rb , in which the qubit in this experiment is based on, is less responsive to frequency shift as a result of static magnetic field as compared to ^{85}Rb clock transition [3,4]. While the $F = 1$ and $F = 2$ transitions are more easily selected within the Rb spectrum, since even in the presence of Doppler broadening, the peaks can be differentiated easily.

B. Initialization (Laser one - 795 nm)

After production and collimation, the atomic beam enters the initialization part of the apparatus (region 1 in Fig. 2 and Fig. 3.b). At this point, the atomic beam interacts with a linearly polarized free space laser beam, approximately 2 mm in diameter and $\approx 1\text{mW}$ power, tuned to D_1 transition of Rb at 794.979 nm using Doppler-Free saturated absorption spectroscopy (DF-SAS). This method of tuning a laser to a given transition is well reported by Preston *et al* [5] and it can easily be reproduced. However, in our experiment we find it is not necessary to have the laser stabilized to the targeted transition. In fact, we find that dithering (injection current modulation method) the laser over a narrow width (70 MHz) surrounding the transition does not only provide a sufficiently stable signal but is far easier to implement. Due to the other time scales used in the experiment (specifically the 75 Hz frequency of the atom beam chopper discussed in section E) this laser is

scanned over this width at the relatively high rate of 10 *KHz*. This means if the transition has a value of ω_0 , instead of stabilizing the laser to ω_0 we choose the laser to scan around ω_0 value with a width of 70 *MHz* and at a speed of 10 *KHz*. This high scanning rate effectively averages the response of the laser over the scanned range, this quasi-lock provided a sufficiently stable signal to observe the microwave qubit manipulation (detailed in section E). The stability of this quasi-lock is dependent on the frequency shift of the External Cavity Diode Laser (ECDL) used in the experiment, which is ultimately dependent on the mechanical and environmental conditions surrounding the ECDL. However, due to the larger width (70 *MHz*) in this quasi-lock condition, the laser center frequency does not require as much readjusting as compared to when the laser is stabilized fully. This is especially important for cheaper diode laser systems where the laser is not thermally controlled. Furthermore, this frequency dithering means that it is not necessary to calibrate for non-perpendicular alignment of the lasers beam and the atomic beam within the chamber. This misalignment leads to a Doppler shift of the transition observed within the atomic beam relative to that observed in the gas cell within the stabilizing setup. This would have to be accounted if the lasers were stabilized.

The laser beam is produced by an ECDL (we used Toptica DL100) and excites the atoms within the beam into one of the short-lived $5^2 P_{1/2}$ excited states. These are not one of the defined qubit states, however with a lifetime of 27 ns the atoms quickly decay back and enter one of the two defined qubit states with approximately equal probability. By pumping only the transition between the $5^2 S_{1/2}: F = 2 \rightarrow 5^2 P_{1/2}$ states it is possible to efficiently transfer the majority of the atoms in the atomic beam into the $5^2 S_{1/2}: F = 1$ qubit state before they leave the laser's cross-sectional area. This method therefore allows for the initialization of the qubits in the atomic beam into a single qubit state regardless of the state they are created in by the source, fulfilling the second criteria.

C. Coherence (Vacuum chamber)

When in use, the chambers are kept at a pressure of 10^{-7} *mBar*, these vacuum conditions increase the mean free path of the atoms and therefore significantly decreasing the probability of decoherence (unlike reference cell where coherence is rapidly lost, the vacuum-like conditions preserve coherence better as compared with reference cells even with buffer gas or anti-relaxation cell wall coating). This increased undisturbed atomic path combined with the very long lifetimes of the rubidium ground states leads to a long coherence time scale compared to the experimental time scale. In this case, the experimental time scale is determined by the time of flight of the atoms between initialization and detection, of order few milliseconds. Therefore, we are able to achieve the first two DiVincenzo criteria using the SAES getters dispenser and by the appropriate choice of physical qubit system. We observe the persistence of the initialized states at the detection stage as shown in Fig. 5, clearly in this setup coherence is maintained.

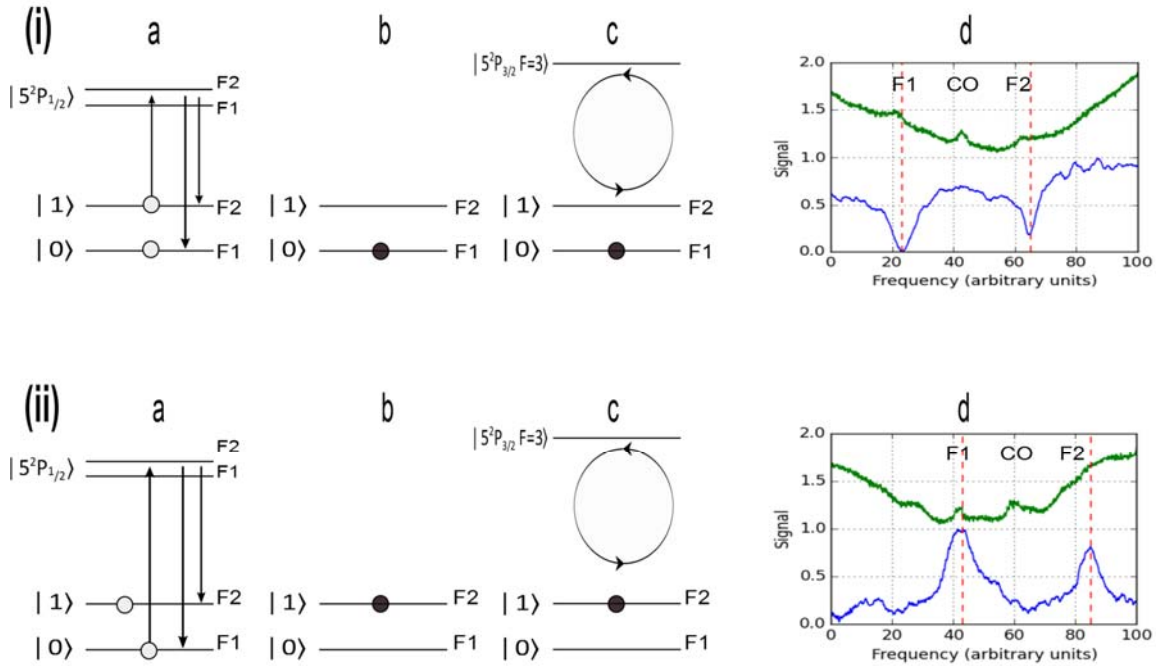


Figure 5. Demonstration of the workings of the initialization and detection system with no microwave manipulation present. The figure shows two different conditions of the initialization for row (i) and (ii) and the subsequent change in the detection signal.

D. State Detection (Laser two - 780 nm)

The final state of the qubits within the atomic beam is read out via a second linearly polarized laser, this time at a wavelength of 780.241 nm (D₂ line) having a radius of 2 mm and a power of ≈ 1 mW. The method of tuning the laser here, is based on polarization spectroscopy (PS) where a detailed experimental setup is reported by Pearman *et al* [6] (for simplicity reasons both lasers could be tuned using DF-SAS, or PS, however, both DF-SAS and PS have been used due to other ongoing experiments, where these two stabilization method were part of the setup). This second laser is produced by a separate ECDL (also Toptica DL100) with its spectral line corresponding to a transition from either of the qubit ground states to the $5^2 P_{3/2}$ excited state, this is another short-lived non-qubit state.

This excited energy level is composed of four hyperfine states with total atomic angular momentums $F=0, 1, 2$ and 3 respectively. Due to the angular momentum selection rules, atoms in $5^2 P_{3/2}: F=3$ can only relax back into $5^2 S_{1/2}: F=2$. By tuning the laser to this closed transition we have a method of photon amplification via direct electron shelving. Atoms entering the detection stage (region 3 in Fig 2) in the $5^2 S_{1/2}: F=2$ state will be excited into $5^2 P_{3/2}: F=3$ and will produce a single photon of measurable light as they relax back into $5^2 S_{1/2}: F=2$. Due to the short lifetime of the excited state, each atom entering $5^2 S_{1/2}: F=2$ will go through multiple excitation/relaxation cycles and will produce 10s of photons before leaving the detection stage. The relative occupation of the qubit states within the atomic beam can then be monitored by observing the fluorescence from this laser interaction. This monitoring fulfils the final detection condition.

The combined initialization and detection systems at work is shown in Fig. 5, where two different cases are considered, these two conditions are represented by row (i) and row (ii) of the figure. The process that is taking place is as follow.

In row (i) of Fig. 5, the initialization laser (795 nm) exciting the transition from the $5^2 S_{1/2}: F=2$ qubit states to either of the short-lived $5^2 P_{1/2}$ states, which have total atomic angular momentum $F =$

1 and $F = 2$, respectively. This indirectly pumps the atoms from $5^2S_{1/2}: F = 2$ into $5^2S_{1/2}: F = 1$, the initialized occupations represented by (i)-b in Fig. 5. For this particular initialization, there are fewer atoms for the detection laser to interact with, Fig. 5 (i)-c, compared to the thermal distribution created by the source. Row (i)-d shows the detection in the form of a signal as the initialization laser frequency is scanned over the $5^2S_{1/2}: F = 2 \rightarrow 5^2P_{1/2}$ Doppler broadened peak, whilst the detection laser is quasi-locked to the transition between $5^2S_{1/2}: F = 2 \rightarrow 5^2P_{3/2}: F = 3$. The top trace (green) is the reference signal from the initialization laser obtained through DF-SAS, the bottom trace (blue) is the fluorescence signal from the detection stage. The $F=1$ and $F=2$ peaks in the reference trace correspond to the transition $5^2S_{1/2}: F = 2 \rightarrow 5^2P_{1/2}: F = 1$ and $5^2S_{1/2}: F = 2 \rightarrow 5^2P_{1/2}: F = 2$ respectively; while CO is a crossover resonance. When the initialization laser is on resonance with one of the transitions, at $F=1$ and $F = 2$, the atoms are initialized almost entirely in $5^2S_{1/2}: F = 1$, at all other frequencies there is a roughly equal population of $5^2S_{1/2}: F = 1$ and $5^2S_{1/2}: F = 2$. This initialization is observed as a decrease in the fluorescence signal from the detection laser at $F = 1$ and $F = 2$.

Row (ii) of Fig.5 shows a similar structure however this time in (ii)-a the initialization laser drives the transition between $5^2S_{1/2}: F=1$ and either of the $5^2P_{1/2}$ excited states. This time, the qubits are pumped into $5^2S_{1/2}: F = 2$ from $5^2S_{1/2}: F = 1$, as seen in (ii)-b, and there is an increase in the number of atoms available for the detection laser to interact with, (ii)-c. In (ii)-d the bottom trace is again the fluorescence from the detection laser which is quasi-locked to the $5^2S_{1/2}: F = 2 \rightarrow 5^2P_{3/2}: F = 3$ transition and the top trace is the saturated absorption spectroscopy reference from of the initialization laser; however, this time, the initialization laser is scanning the $5^2S_{1/2}: F = 1 \rightarrow 5^2P_{1/2}$ Doppler broadened peak. In this case when the initialization laser is on resonance with the atomic transitions ($F = 1$ and $F = 2$) the resulting increase in the population of $5^2S_{1/2}: F = 2$ manifests itself as an increase in the fluorescence from the detection laser. The frequency of this laser is also dithered over a width of 70 MHz about the center frequency of the transition at a rate of 13 KHz (deliberately picked to be different from that of the initialization laser, to avoid the possibility of the lasers scanning in synchronized manner and never simultaneously being on resonance) to negate the need for stabilization.

E. State Manipulation (Microwave - 6.834 GHz)

The manipulation of single qubit states is achieved by interacting the atomic beam with a resonant microwave field before the detection stage (region 2 in Fig. 2). This field is housed in a section of microwave waveguide and drives the Rabi oscillation between the two qubit states. A small hole found on the middle of the cavity let the atoms pass through. Whilst passing the cavity, the atoms interact with the microwave; the effect of this interaction is to directly transfer a fraction of the atoms within the beam back into the $5^2S_{1/2}: F = 2$ qubit states. The length of this interaction is determined by the time of flight (TOF) of the atoms through the waveguide. This is set by the distribution of velocities produced by the source and remains reasonably fixed. On the other hand, the Rabi frequency is a function of the microwave field power; therefore by altering the field power it is possible to tune the post interaction occupation of the qubit states.

Experimentally the resonant frequency was found to be $6.834\ 684\ 240 \text{ GHz}$, this is shifted by 1.63 KHz compared to the reported value of $6.834\ 682\ 610\ 904\ 290(90) \text{ GHz}$ (Ref. [3]), see Fig. 6 for resonance peak. This shift can be accounted for by considering stray static magnetic field within the laboratory as well as imprecision of the equipment used.

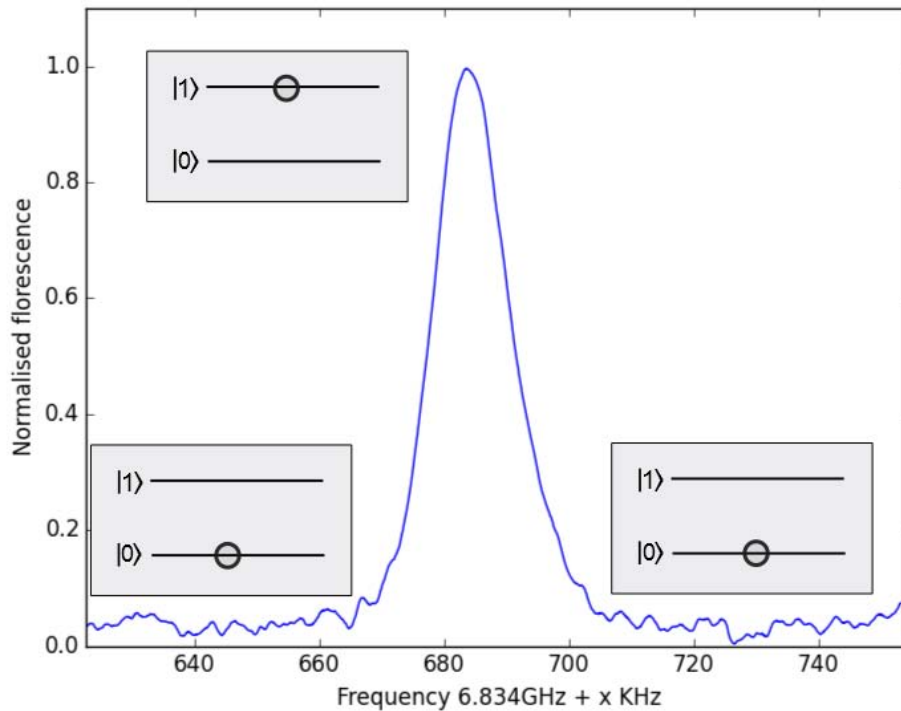


Figure 6. Microwave resonance between $5^2S_{1/2} (F = 1 : m_f=0)$ and $5^2S_{1/2} (F = 2 : m_f=0)$ (this transition was chosen for its second order dependency on the magnetic field, we have made sure this is the chosen transition by first choosing an appropriate microwave power, select the right frequency then detune the frequency around this central value). With both lasers locked to suitable transitions the microwave field frequency was scanned at a rate of 10 KHz/s . The qubits, initialized in $5^2S_{1/2} : F = 1$, then pass through the microwave field and to detection. The trace shows the fluorescence from the detection stage. When the microwave field is off resonance the qubits pass through the field unaffected. The detection laser can only excite atoms from the $5^2S_{1/2} : F = 2$ state (which is unoccupied) therefore we observe minimum fluorescence. When the microwave field is on resonance the field couples with the atomic transition and a fraction of the qubits are transferred directly into the $5^2S_{1/2} : F = 2$ state; this leads to an increase in the number of atoms available for the detection laser to interact with and hence the increase in the fluorescence observed. The normalization of the peak is carried out by subtracting a linear line with the point of minimum amplitude and the resonance was found to have a $FWHM = 12.78 \text{ KHz}$ }

It was found that the signal to noise ratio at the detection stage could be improved significantly by the addition of a 75 Hz tuning fork chopper and a lock-in amplifier (we used *SR850 DSP*) as it can be seen from Fig.7 (the tuning fork is found at position *h* in Fig. 2). The chopper was positioned such that the knife-edge plates were within 5 mm of the beams entrance hole into the microwave waveguide. Whilst chopping, the knife edge plates on the arms of the tuning fork changes sinusoidally between being separated by 4 mm and completely overlapping. Whilst open, the entire width of the atom beam could pass uninterrupted however when overlapping the beam was completely blocked. Because of this it was important to ensure that none of the interesting dynamics could be contained completely within this downtime. This was achieved ensuring that the scan rate of the first laser was slow enough such that each resonance peak was chopped into numerous pieces and not fully contained within the period the atom beam was blocked. A scan rate of 0.1 Hz was found to give a good resolution.

At 75 Hz the intensity of the atomic beam is modulated relatively slowly by the chopper, as a result, it is necessary to sweep the microwave field over a long time scale in order to measure the resonance curve. Scanning the microwave field frequency at a rate of 10 KHz/s is sufficiently slow to produce the resonance peak in Fig. 6. Through this microwave interaction, we are able to achieve

single qubit state manipulation.

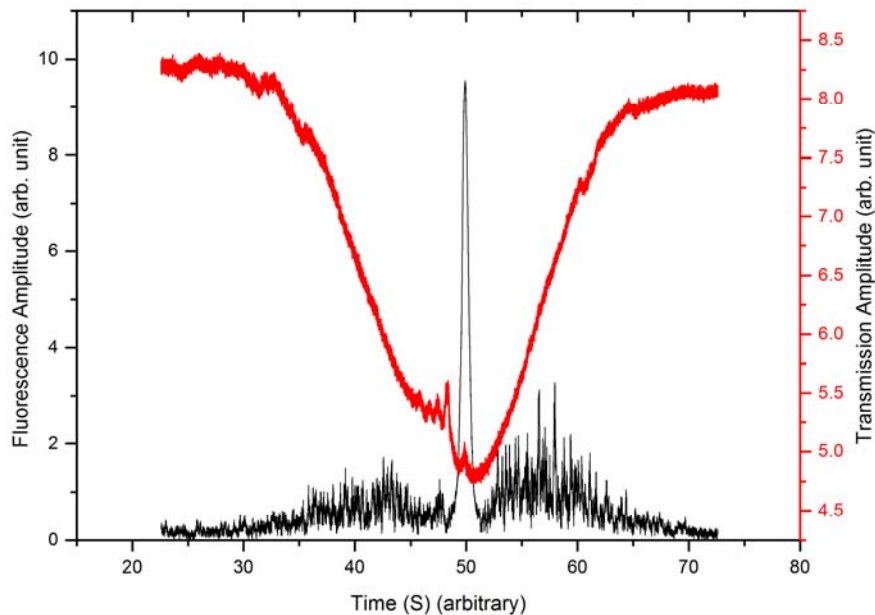


Figure 7. Improvement of the signal to noise ratio via the addition of a tuning fork to the experimental setup. The chopper was placed in front of the waveguide (position *h* in Fig.2). Here a test is carried out on $^{85}\text{Rb-D}_2$ line in red to select a given transition as chosen by the user. The test was to check if a given transition can easily be selected and how much the signal can be improved. An improvement of two orders of magnitude is seen in black because of the addition of the tuning chopper.

For a viable quantum computer (as required by the criteria in the introduction), a universal set of quantum gates is needed. Implementing this requires a method to interact multiple qubit states together. Similar multiple atomic qubit interactions have already been achieved within cavity QED experiments [7]. Within these experiments, the near impossible task of entangling two atoms in a free space collision is simplified by coupling them simultaneously or, in fact, sequentially to a macroscopic cavity. This step, however, could not be achieved within the framework of this experiment. This was mainly due to the large size of the chamber and the large number of atoms within the atomic beam.

4. Conclusion

We have presented a detailed experiment that demonstrates atomic state manipulation, which can be translated to qubit manipulation. To make this possible we have utilized a number of simplifying techniques. Firstly using a SAES getters alkali metal dispenser and collimating aperture we have been able to reliably create an atomic beam without the use of complicated oven systems. Secondly, by appropriate choice of initialization and detection transitions, we have ensured we have a strong signal easily observable with an over-the-counter photodiode. This signal can be further improved by the addition of a tuning fork chopper and lock-in amplifier. Finally, we have recognized that a scanning function generator, which is already easily used to observe atomic spectra, can be used to achieve a quasi-lock with sufficient stability within the scope of this experiment. This quasi-lock negates the need for more complicated locking procedures.

Finally, we would like to emphasize that the experimental setup we have presented here has many other applications within various fields of physics and therefore it is by no means a single-use experiment. For example, the setup can be taken advantage of and used in the field of atomic clocks,

principles of Rabi frequency, various atom-light interaction such as Coherence Population Trapping (CPT) and investigation of Breit-Rabi approach to atom-magnetic field interactions (both in weak and intermediate external magnetic fields). We leave the reader to explore many possible additions to this setup, however, a good starting point would be the exploration of any of these works [8–12].

References

- [1] T. Sleator and H. Weinfurter, *Phys. Rev. Lett.* **74**, 4087 (1995).
- [2] D. P. DiVincenzo, *Fortschr Phys.* **48**, 771 (2000).
- [3] D. A. Steck, Rubidium 87 D Line Data Available Online [Http//steck.us/alkalidata](http://steck.us/alkalidata) (2010).
- [4] D. A. Steck, “Rubidium 85 D Line Data” Available Online [Http//steck.us/alkalidata](http://steck.us/alkalidata) (2013).
- [5] D. W. Preston, *Am. J. Phys.* **64**, (1996).
- [6] C. P. Pearman, C. S. Adams, S. G. Cox, P. F. Griffin, D. a. Smith, and I. G. Hughes, *J. Phys. B At. Mol. Opt. Phys* **35**, 5141 (2002).
- [7] S. Osnaghi, P. Bertet, A. Auffeves, P. Maioli, M. Brune, J. M. Raimond, and S. Haroche, *Phys. Rev. Lett.* **87**, 37902 (2001).
- [8] M. Arditi and J. L. Picqué, *J. Phys - Paris* **41**, 379 (1980).
- [9] M. Arditi and P. Cerez, *IEEE T. Instrum. Meas* **21**, 391 (1972).
- [10] C. Liu and Y. Wang, in *2013 Jt. Eur. Freq. Time Forum Int. Freq. Control Symp. EFTF/IFC 2013* (2013), pp. 761–763.
- [11] J. Vanier, *Appl. Phys. B* **81**, 421 (2005).
- [12] R. C. Mockler, *Atomic Beam Frequency Standards* (1961).